Tautomeric Forms of 2-Thiobarbituric Acid As Studied in the Solid, in Polar Solutions, and on Gold Nanoparticles

ARTICLE *in* THE JOURNAL OF PHYSICAL CHEMISTRY C · MARCH 2007

Impact Factor: 4.77 · DOI: 10.1021/jp0628176

8 AUTHORS, INCLUDING:

Eduardo Méndez
University of the Republic, Uruguay
46 PUBLICATIONS **510** CITATIONS
SEE PROFILE

Jorge S. Gancheff
University of the Republic, Uruguay
45 PUBLICATIONS **337** CITATIONS
SEE PROFILE

Jorge Castiglioni
University of the Republic, Uruguay
21 PUBLICATIONS **210** CITATIONS
SEE PROFILE

Oscar N. Ventura
University of the Republic, Uruguay
115 PUBLICATIONS **1,395** CITATIONS
SEE PROFILE

Tautomeric Forms of 2-Thiobarbituric Acid As Studied in the Solid, in Polar Solutions, and on Gold Nanoparticles

Eduardo Méndez,*,† María F. Cerdá,† Jorge S. Gancheff,‡ Julia Torres,‡ Carlos Kremer,‡ Jorge Castiglioni,§ Martina Kieninger,|| and Oscar N. Ventura*,||

Laboratorio de Biomateriales, Instituto de Química Biológica, Facultad de Ciencias, Universidad de la República, Iguá 4225 casi Mataojo, 11400 Montevideo, Uruguay, and Departamento Estrella Campos and DETEMA, Facultad de Química, Universidad de la República, Casilla de Correo 1157, Montevideo, Uruguay

Received: May 8, 2006; In Final Form: October 24, 2006

2-Thiobarbituric acid (TBA) coated gold nanoparticles (average diameter = 5.90 nm) were produced and studied by several experimental and theoretical methods. As part of this study, the molecular structure of TBA tautomers in the solid, in polar solutions, and adsorbed onto gold nanoparticles was studied. The resolution of this complicated system (10 possible isomers) was accomplished with the aid of experimental (IR, UV−vis, and NMR) and theoretical (DFT and MP2) methods. The general conclusion is that there are two preeminent isomers, N1 and N10, with different stabilities in different media. N1, the keto−thione tautomer, is the most stable in gas phase ($\Delta G^{o}_{298} \approx 8-9$ kcal/mol lower than the second-most stable isomer, depending on the method of calculation used). However, experimental spectroscopic data supported by the theoretical calculations strongly suggest an equilibrium between the tautomers N1 and N10 in methanol solution, where enolization of one keto group is produced by proton transfer from the methylene group, which is more acidic than the NH groups. With the use of the polarizable continuum method for simulating solvents, N10 is predicted to be even more stable than N1 by $\Delta G^{o}_{298} \approx 1$ kcal/mol in methanol. On the other hand, the IR spectrum of the solid can be best explained by assuming that only N10 is present, a fact also supported by the observation that the IR spectrum of TBA absorbed onto gold nanoparticles can be explained by a larger ratio of [N10]/[N1] than that present in methanolic solution. Isomerization of N1⇌ N10 can be explained by intervention of the solvent, proceeding faster in methanol solutions than in DMSO, where it is nevertheless observed after a time, according to the ^{13}C NMR spectra. Our experiments support absorption of TBA onto gold nanoparticles through S−Au and N−Au interactions, with the preeminence of a N10-like enol structure. The experiments also demonstrate that the synthesized TBA-coated gold nanoparticles can autoassociate by hydrogen bonding to form larger structures. This same H-bonding capacity also assures that these coated nanoparticles act as thistles toward proteins in solution, binding them strongly, presumably not by chemical reaction but by a network of hydrogen bonds.

Introduction

The electrochemistry of redox proteins is usually studied through a suitable electrode covered with an appropriate ω-functionalized alkanethiol monolayer, which in turn interacts with the protein residues through van der Waals and/or electrostatic interactions.[1−5] Although such platforms have provided good response in terms of protein adsorption, the electron transfer across the monolayer corresponds to a nonadiabatic regime, and it is strongly dependent on the thiol chain length.[6,7]

In view of this situation, new platforms have been proposed in order to shorten the electron pathway and turn the electron-transfer process into the adiabatic regime. Adsorption of N-heterocyclic thiols provides a good approximation to achieve this goal,[8,9] acting at the same time as electron-transfer promoters toward protein electrochemistry.[10−14] However, the use of these compounds brings up new problems, namely, the existence of tautomeric equilibriums due to the presence of mobile H atoms[9,14−17] and the existence of polymorphism in the solid.[18−20]

Several experimental methodologies can be applied for the identification of the tautomeric forms: IR spectroscopy provides easily recognizable adsorption bands for functional groups,[16,21,22] UV−vis absorption spectroscopy has been shown to be a valuable tool in the distinction of thione−thiol tautomers,[15,17] and ^{1}H and ^{13}C NMR spectroscopies yield further evidence for structural features.[17,23] Regarding the adsorbed state, the development of monolayer-protected gold clusters has been successfully used as a model system for self-assembled monolayers on planar surfaces,[24] with the benefit that bulk spectroscopies applied for their characterization can be equivalently used as surface spectroscopic techniques.[23,25]

2-Thiobarbituric acid (TBA) is a substituted mercaptopyrimidine with 3 mobile H atoms and 10 possible tautomeric forms (Chart 1). TBA appears as a suitable candidate for self-assembling onto gold, and its ability to form N,S-coordinated complexes with Au(I) as well as supramolecular structures through N−H···O and C−H···O bonds has already been

* Corresponding authors: E. M. (for experimental aspects), e-mail: emendez@fcien.edu.uy. Tel: +5982-5250800. Fax: +5982-5258617. O. N. V. (for theoretical aspects), e-mail: onv@fq.edu.uy. Tel: +5982-9248396. Fax: +5982-9241906.

† Laboratorio de Biomateriales, Facultad de Ciencias.

‡ Departamento Estrella Campos, Facultad de Química.

§ LAFIDESU-DETEMA, Facultad de Química.

|| CPG-DETEMA, Facultad de Química.

10.1021/jp0628176 CCC: $37.00
Published on Web 02/02/2007

CHART 1: Possible Tautomeric Forms of 2-TBA Acid[a]

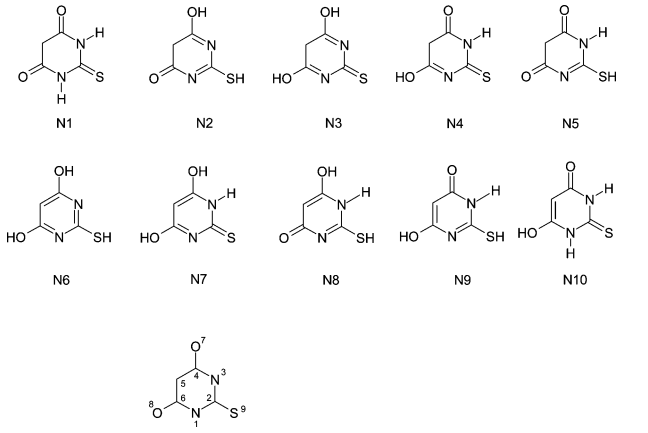

[a] Each one was named after Zucarello et al.[33] The numbering system used throughout this work is indicated in the bottom structure.

demonstrated.[26] However, previous reports on TBA adsorption have not taken into account the existence of the different tautomeric forms.[27,28] There are few reports on the spectroscopic characterization of TBA[29,30] and TBA derivatives,[26,31] and signal assignments, especially from NMR spectroscopies, are somewhat contradictory.[29,32] Due to the high number of possible tautomers and the obvious lack of them in a pure form to compare experimental spectra, it is necessary to supplement the experimental work with reliable computations. In this sense, density functional theory (DFT) was shown to yield good predictions for UV−vis, IR, and NMR spectra regarding thione−thiol tautomerism.[17,33,34]

The correct identification of the tautomeric forms of TBA in the solid, in solution, and adsorbed onto gold nanoparticles appears as a challenging task due to the inherent complexity of the system under study. To accomplish such an objective, we employed UV−vis, IR, and ^{1}H and ^{13}C NMR spectrosocopies with the aid of DFT and MP2 calculations for signal assignments. TBA-capped gold nanoparticles were reproducibly synthesized in good yield by addition of $NaBH_4$ to a methanolic solution of TBA and $HAuCl_4$. Thermal gravimetric analysis (TGA), transmission electron microscopy (TEM), and scanning electron microscopy (SEM) coupled with electron dispersive spectroscopy (EDS) were used for further characterization of this system. The conclusions were that TBA is present in two tautomeric forms at equilibrium in methanol solution (N1 and N10, Chart 1), that the enol form N10, formed by solvent-assisted transfer of one of the most acidic CH_2 protons, is the isomer binding preferentially to the Au clusters, and that these nanoparticles (with an average diameter of 5.90 nm) act like thistles to each other forming larger aggregates by mutual multiple hydrogen-bonding interactions.

Experimental Section

Chemicals. Sodium borohydride (99%, Aldrich), hydrogen tetrachloroaurate(III) trihydrate (98%, Aldrich), and 2-TBA acid (98%, Merck) were used as received. Ultrapure water (resistivity >18 MΩ cm^{-1}) was obtained from a MilliQ purification system. All other solvents were of HPLC grade and were dried with molecular sieves before using.

Fourier Transformed Infrared Spectroscopy (FTIR). Solid-state IR spectra were recorded on a Bomen FTIR spectrophotometer as 1% KBr pellets. Samples of solutions were measured in a spaced-window cell with a plane-faced NaCl window.

CHART 2: Isomeric Structures of Mono- and Dianions of TBA Obtained from the Neutral Isomers N1 and N10

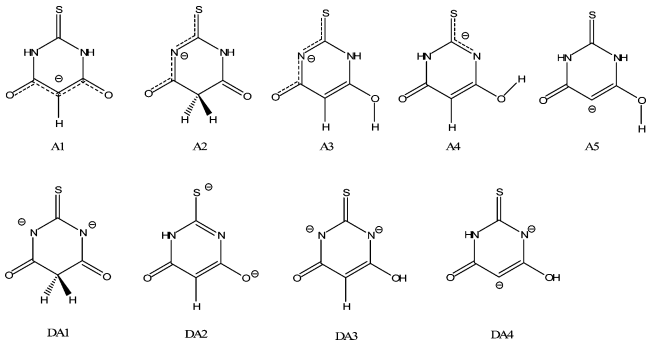

UV−vis Spectroscopy. UV−vis spectra were obtained in a Shimadzu UV-1603 UV−vis spectrophotometer. Solution spectra were obtained by measuring the absorption of dilute solutions in a quartz cell with a path length of 1 cm.

Nuclear Magnetic Resonance. A Bruker Avance 400 DPX spectrometer was employed for the acquisition of nuclear magnetic resonance spectra of TBA in dried DMSO solutions. ^{1}H NMR spectra were obtained immediately, and ^{13}C NMR spectra were obtained in the same solution within 2 days, in order to get good signals.

Theoretical Calculations. Second-order Møller-Plesset[35] and DFT[36] (PBE[37] and B3LYP[38]) methods were employed to perform the theoretical calculations. Several basis sets including Pople's[39] 6-31G(d), 6-311G(d,p), and 6-311++G(2df, 2pd) and Dunning's[40] aug-cc-pVTZ were employed in different stages of the calculations. Geometry optimizations were performed both in vacuum and using the polarizable continuum method (PCM) of Tomasi et al.[41] Neutral species for all tautomeric forms (Chart 1) were considered, and the most stable conformer was used in case several of them were possible. Some mono- and dianions of the most stable isomers N1 and N10 were also studied at the PBE/6-311++G(2df,2pd) level. Their structures are depicted in Chart 2. Critical points were characterized by the number of negative eigenvalues of the Hessian. Infrared frequencies and intensities for the transitions were obtained within the harmonic approximation, and the frequencies were scaled with appropriate multiplicative factors depending on the method of calculation to obtain fundamental transitions comparable to those of experimental measurement. UV−vis transitions were obtained employing time-dependent density functional methods (TD-DFT[42]). NMR[43] spectra were also calculated theoretically, employing the GIAO method.[44] Several dimers of isomers N1 and N10 with themselves were also studied. Their structures are depicted in Chart 3. Geometry optimization was performed in the same way as for the monomers but using the smaller B3LYP/6-311+G(d,p) chemical model instead of the larger one. Due to the use of a relatively modest basis set in this case, stabilization energies were corrected for basis set superposition error (BSSE) by applying the usual counterpoise correction.[45] The *Gaussian 03*[46] system of programs was used for the calculations presented in this paper (ca. 200). Calculations were performed in an SGI Altix server equipped with 1500 MHz Itanium2 processors, using eight processors per individual run.

Synthesis of TBA-Capped Gold Nanoparticles. The synthesis of surface-functionalized colloidal gold particles was performed by the single-phase method.[47] Briefly, $HAuCl_4 \cdot 3H_2O$ and TBA methanolic solutions were mixed in a molar ratio of 1:2, and a 10-fold molar excess of solid $NaBH_4$ was added while the mixture was being vigorously stirred. There was an immediate color change of this solution from yellow to black,

CHART 3: Structure of the $(N1)_2$ and $(N10)_2$ Dimers Studied in This Work

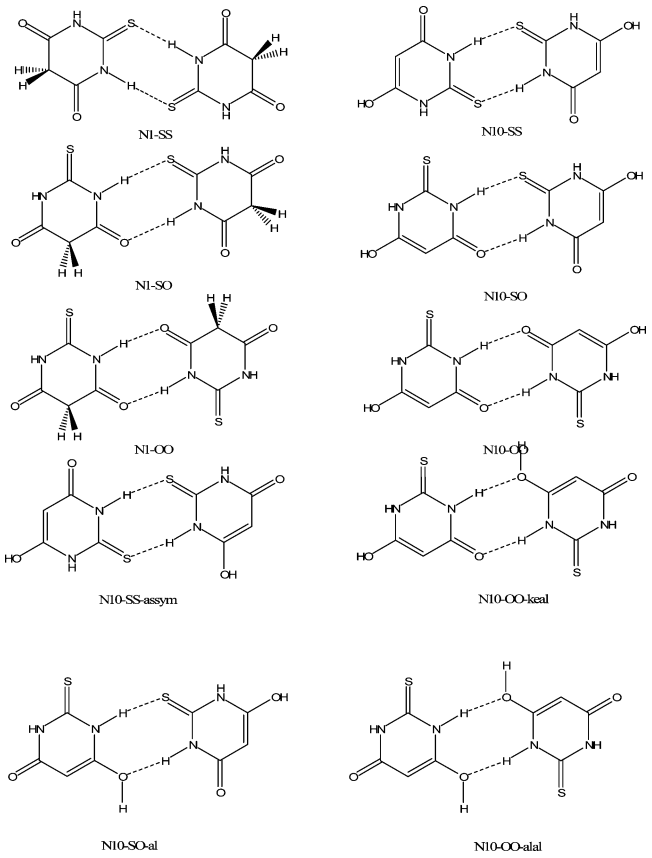

and the solution was left at room temperature while it was continually stirred for 3 h to achieve thermodynamic equilibrium. The resulting product precipitated immediately upon addition of $NaBH_4$. After completion of the procedure, the solution was centrifuged at 5000*g* and resuspended in diethyl ether and water to remove excess materials.

Potentiometric Titrations. Protonation constants of TBA were determined through three potentiometric titrations (ca. 150 experimental points each) in the concentration range of 3 to 10 mM, covering pH values between 2 and 11. In all cases, the solutions were poured into a 50 mL titration cell together with a known amount of 0.1 M NaOH. After thermal equilibrium was reached, hydrogen ion concentrations were determined in successive readings, each performed after a small incremental addition of standard 0.1 M HCl solution (carried out with the help of a Crison 2031 piston buret). Electromotive force values were recorded with the help of a Radiometer 85 pH meter, using a glass electrode and a calomel reference electrode. Ionic strength was kept constant throughout the titrations by using solutions containing 0.15 M NaCl. Presaturated CO_2-free Ar was bubbled through the solutions during titrations to eliminate the effect of atmospheric carbon dioxide, and the temperature was kept at 25.0 (±0.1) °C. The cell constants $E°$ and the liquid junction potentials were determined according to the methods of Biedermann and Sillén[48] and Liberti and Light.[49] Data were analyzed using the HYPERQUAD program,[50] and species distribution diagrams were produced using the HySS program.[51] The fit of the values predicted by the model to the experimental data was estimated on the basis of the parameter σ.

Transmission Electron Microscopy (TEM) and Electron Dispersive Spectroscopy (EDS) Analyses. Bright-field images were obtained in a JEOL JEM-1010 TEM operating at 100 kV.

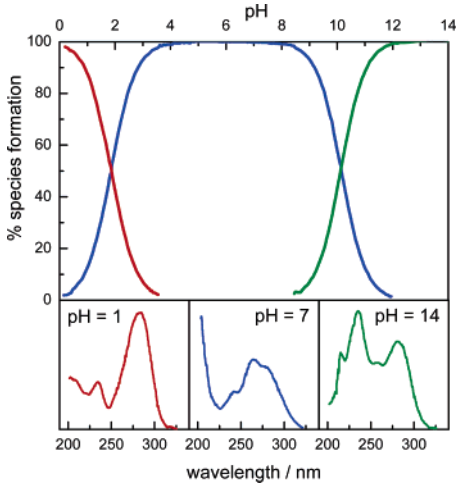

Figure 1. TBA species distribution diagram as a function of solution pH (top) and the corresponding UV−vis spectra (bottom).

The samples were prepared by placing a dilute chloroform solution of the TBA-capped gold nanoparticles onto 300-mesh carbon-supported film copper grids and allowing the solvent to evaporate. The particle sizes were determined using Image J software.[52] EDS analysis was performed in the SEM environment using a JEOL JSM-5900 LV coupled with EDS Vantage Thermo Noran equipment.

Thermogravimetric Analysis (TGA). TBA-capped gold nanoparticles aggregates were analyzed in a Shimadzu TGA-50 equipment. Samples (9 to 14 mg) were placed in platinum capsules under dried air (99.9%) at a flow rate of 50 mL min^{-1}. A programmed temperature, including a holding step at 103 °C for 30 min, followed by a temperature increase at 0.5 °C min^{-1} up to 700 °C, was used. Differential thermogravimetric profiles (DTGA) were obtained by graphical differentiation of the TGA register.

Results

Acid−Base Properties of TBA. The neutral molecule HTBA can be protonated or deprotonated depending on the pH value.[33] The pK_a values we found for the processes are

$$\mathrm{HTBA} \rightleftharpoons \mathrm{H^+ + TBA^-} \quad \log K_1 = -10.16(1)$$

$$\mathrm{HTBA + H^+} \rightleftharpoons \mathrm{H_2TBA^+} \quad \log K_2 = -1.874(8)$$

With these values, the speciation of the system (Figure 1) shows the predominance of a cationic species at low pH values, a neutral species between pH 4 and pH 8, and an anionic species at high pH values. With this diagram and recording the UV−vis spectra at those pH values where a single species predominates (Figure 1, bottom), it is possible to assign a pure spectrum for each species. Maximal wavelength values are 235 and 283 nm (pH = 1), 242 and 264 nm (pH = 7), and 235, 252, and 283 nm (pH = 14).

Theoretical Calculation of the Structure and Stability of TBA Isomers. Geometry optimization of the ten TBA isomers shown in Chart 1 was performed at the B3LYP, PBE, and MP2 level using several basis sets up to 6-311++G(2df,2pd). Smaller basis sets and the comparable aug-cc-pVTZ basis set were used in gas-phase calculations to assess the precision of the results. Total energies at the different theoretical levels are given in Table SM1 in the Supporting Information. Relative energies with respect to the most stable isomer N1 are shown in Table 1. If a reasonably large basis set is used, no significant difference

TABLE 1: Gas-Phase Relative Energies (in kcal/mol) of TBA Isomers with Respect to the Most Stable One (N1) Using Different Chemical Models[a]

	B3LYP				MP2	
isomer	6-31G(d)	6-311G-(d,p)	6-311++G-(2df,2pd)	aug-ccp-VTZ	6-31G(d)	6-311++G-(2df,2pd)
N1	0.0	0.0	0.0	0.0	0.0	0.0
N2	32.1	31.2	29.3	29.2	33.4	29.0
N3	36.0	34.2	33.1	32.9	36.0	31.1
N4	16.9	16.1	15.4	15.3	17.6	14.9
N5	21.3	20.9	19.4	19.3	21.0	19.1
N6	19.2	15.0	12.5	12.3	19.9	9.5
N7	25.3	21.3	19.6	19.2	27.8	18.6
N8	34.6	31.2	27.8	27.6	36.2	26.6
N9	20.1	16.6	13.8	13.7	22.0	13.0
N10	12.4	9.0	7.7	7.5	14.3	7.6

[a]Total energies are given in Table SM1 in the Supporting Information.

is observed between DFT and MP2 calculations. Even the results obtained at the relatively modest B3LYP/6-311G(d,p) level are comparable to those at the more costly MP2/6-311++G(2df,-2pd) level.

Large basis set calculations were performed in gas phase and simulated chloroform, methanol, and dimethylsulfoxide solvation using the PCM method. Geometry optimization and Hessian calculations were performed in the field of the solvent, if any. Total free energies at 298 K are reported in Table SM2 in the Supporting Information, whereas relative free energies with respect to isomer N1 are shown in Table 2. The main results are that the methods employed are convergent with respect to the increase of the basis set size and that N1 is the most stable isomer in gas phase for all methods used. However, solvation strongly affects this stability pattern, because of the stabilization of isomers of large dipole moment (whereas N1 has a dipole moment of 0.23 D in gas phase, according to PBE/6-311++G-(2df,2pd) calculations, and N10 has a dipole moment of 5.05 D). In particular, isomer N10 becomes even more stable than N1 in methanol at the three levels of calculation.

Infrared Spectra of TBA. The vibrational spectrum for solid TBA dispersed in pellet KBr is shown in the range of 4000−300 cm^{-1} in Figure 2a. The absence of the characteristic band attributed to the stretching vibration of the −SH group at 2300−2500 cm^{-1} and the presence of the signal corresponding to a cyclic thioamide structure −NH-(C═S) at 1567 cm^{-1} indicate that a thione form prevails in the solid state. In addition, the characteristic bands for carbonyl group in a β-unsaturated position at 1716 and 1647 cm^{-1} are in agreement with the presence of the N10 isomer in the solid state. Therefore, the calculated IR spectrum of this isomer was compared to the experimental one to confirm and complete the band assignments (Table 3). Approximate fundamental frequencies were obtained from the calculated harmonic frequencies for the monomer in gas phase by employing the usual scaling factors. B3LYP, PBE, and MP2 calculations exhibit a reasonable agreement among themselves and with experiment except for the bands corresponding to hydrogens presumably involved in interchain hydrogen bonding in the solid.

ν(N−H) bands are theoretically predicted in the interval of 3430−3500 cm^{-1}, depending on the method of calculation. Only one of these bands is observed experimentally, implying that one of the N−H bonds is not free but forming a hydrogen bond. Similarly, the free ν(O−H) band predicted in the interval of 3670−3690 cm^{-1} is not present in the experimental spectrum, implying also that this H is participating in a hydrogen bond (simple molecular modeling of a simulated N10 solid shows that this H atom should be involved in interchain interactions with the sulfur of a proximal chain). In this regard, the band observed at 2873 cm^{-1}, not predicted theoretically, could be attributed to hydrogen bonding to S and O.[26,30] Signals corresponding to C_5−H vibrations are seen in the experimental spectrum, suggesting that this hydrogen does not participate in intermolecular interactions in the solid.

Several hydrogen-bonding patterns are possible for isomer N10 in the solid. A full analysis of the solid at a reasonable computational level is outside our present computing capabilities. Therefore, we chose to determine only the vibrational frequencies of some of the dimers which can be formed from N10 using the B3LYP/6-311G(d,p) chemical model. The species studied are depicted in Chart 3 for both N1 and N10. Counterpoise-corrected interaction energies (shown in Table 4) are the lowest for the dimers exhibiting two N−H···O═C or one N−H···O═C and one N−H···S═C hydrogen bond. Although in gas phase the N10 dimers are all less stable than N1 dimers, as happened for the N10 and N1 monomers, dimerization of N10 releases more energy than dimerization of N1 (−9.9 vs −9.1 kcal/mol). This is a suggestion that if both isomers N1 and N10 coexist in solution, nucleation to form the solid could favor N10, thus leading this isomer to be present preferentially in the solid. Moreover, the dimers N10−SO and N10−OO release almost the same amount of energy, suggesting the possible presence of more than one bonding pattern in the solid (polymorphism).

Interesting fundamental frequencies (obtained multiplying by the scaling factor 0.9610) are shown in Table 5 for the N10−OO and N10−SO dimers. The ν(NH) stretching frequency of the non-hydrogen-bonded NH is slightly shifted (12 cm^{-1}) whereas that of the hydrogen bound NH is lowered by about 300 cm^{-1} with respect to the value in the free gas-phase N10 isomer. The ν(NH···O) frequency appears about 90 cm^{-1} below the ν(NH···S) frequency in N10−SO, the latter in the same area as the CH frequencies. The ν(NH···S) transition is the most intense in N10−SO, appearing at about 3159 cm^{-1}. The ν(NH···O) transition is also strong, and both of them contribute to the band around 3000 cm^{-1} that is observed in the spectrum of the solid (Figure 2a) and absent in solution or in the gold-capped nanoparticles (Figure 2, parts b and c). Several strong and medium intermolecular interaction bands are also calculated in the 1500−1750 cm^{-1} region, very much in agreement to those observed experimentally. Since none of the studied dimers involves hydrogen bonding of the OH group, we cannot predict the frequency shift for the OH stretching. Compared to the well-known case of methanol, where the frequency shift from monomer to dimer and up to the liquid has been determined, it is reasonable to assume that this frequency is within the broad band observed between 2500 and 3100 cm^{-1}. At any rate, the absolute intensity of this band would be small, and complexation reduces its intensity even more, probably making it unobservable.

Several differences are present in the methanolic solution IR spectra of TBA in comparison with the one of the solid (Figure 2b). Signals for the cyclic thioamide group and for the carbonyl group in a β-unsaturated position are shifted to lower frequencies. A strong band at 1630 cm^{-1} corresponding to ν(C═O) is observed occupying the place where the intermolecular bands involving the NH groups were present in the solid. All the contributions presumably related to intermolecular interactions in the solid (according to the discussion above for the dimers) are absent. The latter is also evident through the presence of several bands corresponding to N−H bond vibrations at 671 cm^{-1} and most noticeable for ν(N−H) at 2921 cm^{-1}. The OH bands seen at 3380 and 3443 cm^{-1} are probably due to the

TABLE 2: Relative Free Energies (at 298 K and 1 atm, in kcal/mol) of TBA Isomers with Respect to N1 Using Different Methods and the 6-311++G(2df,2pd) Basis Set[a]

	PBE				B3LYP				MP2			
isomer	gas	CHCl3	CH3OH	DMSO	gas	CHCl3	CH3OH	DMSO	gas	CHCl3	CH3OH	DMSO
N1	0.0	0.0	0.0	0.0	0.0	0.0	0.0	0.0	0.0	0.0	0.0	0.0
N2	26.5	26.9	24.7	24.6	25.7	25.5	25.5	25.8	25.9	26.2	25.7	25.2
N3	32.1	30.0	26.4	27.8	32.7	30.4	27.4	28.2	31.0	29.1	27.4	27.1
N4	15.1	14.7	12.4	13.9	15.4	13.5	12.9	13.8	14.0	13.2	13.9	13.5
N5	16.7	16.4	14.1	15.9	16.7	16.2	14.2	15.3	15.7	16.4	15.9	15.8
N6	12.3	12.9	11.0	12.6	11.5	12.4	11.2	12.2	7.6	8.1	7.5	7.2
N7	20.2	13.3	7.9	7.8	20.4	13.2	8.4	9.0	18.6	11.3	7.1	6.5
N8	25.8	19.6	14.4	16.0	25.6	19.5	14.9	15.8	23.5	17.6	13.9	11.9
N9	12.3	10.5	7.7	9.2	12.4	10.6	8.4	9.3	10.7	9.0	7.6	7.2
N10	8.9	3.5	-0.6	0.7	8.7	3.3	-0.2	0.5	7.6	2.5	-0.1	-0.7

[a]Differences in the solvent include both the free energy of the solute and the free energy of solvation. Total free energies are given in Table SM2 in the Supporting Information.

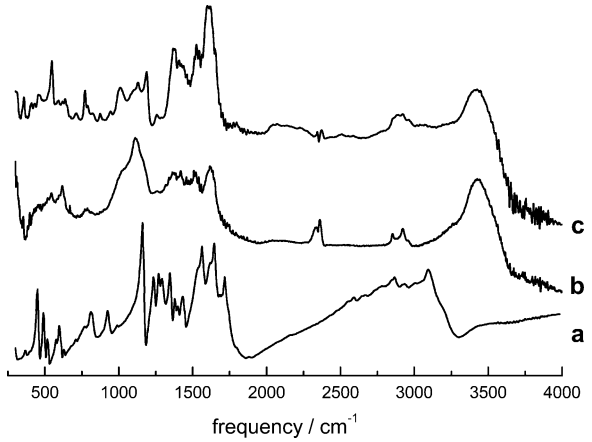

Figure 2. FTIR spectra for (a) solid TBA, (b) methanolic TBA solution, and (c) adsorbed TBA onto gold nanoparticles.

hydroxyl groups in the solvent molecules directly coupled to N10 and not to the hydroxyl in N10 itself. The presence of a CH_2 group is evident through signals at 2853 cm^{-1} (stretching) and 991 cm^{-1} (rocking). Finally, the strong signals at 1510−1539 cm^{-1} are mainly attributed to the thioamide scissoring vibration. Since all these features cannot be explained by the presence of any single isomer, we adopted the hypothesis that a mixture of isomers is present in methanol solution. Together with the calculated fundamentals for N1 and N10, data for the IR transitions in methanol are shown in Table 6 .

To obtain a deeper theoretical insight into the IR spectrum in methanol solution, we performed DFT calculations involving two or four methanol molecules in different positions for the more stable isomers N1 and N10. The optimum structures considered are shown in Figure 3. Calculations were performed in gas phase and simulate methanol as the solvent employing PCM. The results for the relative free energies are shown in Table 7, and the vibrational frequencies are also shown in Table 6. The main result is that methanol preferentially solvates the CH_2 tail of TBA isomer N1. The interaction with the solvent produces calculated vibrations in the region between 2700 and 3000 cm^{-1} which are not calculated in either the isolated molecule or the molecule within the SCRF. Our calculation in the model cluster in methanol produces a band at about 2738 cm^{-1} due to the interaction of the CH_2 in N1 with the solvent and another at 2665 cm^{-1} due to the interaction of the hydroxyl group in N10 with methanol. Since a band is experimentally observed at 2853 cm^{-1}, this is a confirmation that the solvent interacts strongly with TBA. Puzzling signals appearing at 2327-(w) and 2361(s) cm^{-1} are attributed to the blue-shifted coupled C═O stretching vibration. The red-shifted component should appear around 1340 cm^{-1}, where there is also a band due to NH in-plane bending in N1.

The IR spectrum of adsorbed TBA on gold nanoparticles resembles that obtained in methanol, with a few important modifications (Figure 2c). A comparison of the experimental data with those signals calculated in gas phase is shown in Table 8. In particular, part of the signals between 1000 and 1200 cm^{-1} disappear. This is a strong indication of a bound sulfur atom in the adsorbed entity. Moreover, a very strong signal is observed in the fingerprint zone, around 617 cm^{-1}, indicative of a single-bonded C−S group, again reinforcing the idea that TBA is bound to gold through the sulfur atom. This signal is obviously absent in the gas-phase calculation, but experimentally the R_1R_2-HC−S stretching is found between 600 and 630 cm^{-1}.[53] Other signals observed in the solution spectra are also absent, mostly related to NH vibrations. For instance, the free NH wagging calculated in gas phase at 652 cm^{-1} is not detected. The same is true for the band calculated at 1695 cm^{-1}, corresponding to a CNH bending, completely absent in the experimental spectrum and thus supporting the view that there is no proton left over nitrogen in the TBA-capped gold nanoparticles. In addition, ring stretching vibrations are weakened, suggesting a more rigid structure of the adsorbate. Taken together, they indicate the presence of a twice deprotonated TBA isomer interacting "head-on" through the sulfur and one of the nitrogen atoms with the gold atoms in the nanoparticle. Residual CO_2 bands are observed at 2341−2363, 1385, and 636 cm^{-1}. The fact that this last vibration is observed at all, whereas it is IR silent in the gas phase, indicates that CO_2 is bound to the TBA coating of the gold nanoparticle.

UV−vis Spectra of TBA. The UV−vis spectrum of TBA was studied in methanol, both free and absorbed onto gold nanoparticles (Figure 4). Time-dependent DFT calculations of the spectra were performed in vacuum and in different solvents. The most intense electronic transitions are collected in Table 9.

The UV−vis spectra of TBA in methanol (Figure 4, solid line) show an intense band at 283 nm, with a well-defined shoulder at 265 nm and less-defined absorption bands at 244 and 227 nm. These bands cannot be explained at the theoretical level by any one isomer, thus indicating the presence of a mixture as also suggested by the IR spectra. According to what we described before, we felt justified in assuming that both isomers of N1 and N10 are present in methanol solution in approximately the same concentration. We then performed a simulated UV−vis spectrum considering the addition of the theoretical spectra of N1 and N10. The comparison with the experimental spectrum in methanol is shown in Figure 5a. The error between the

TABLE 3: FTIR Signals for Solid TBA and Calculated for N10 Tautomer[a,b]

	calculated N10 tautomer[a]			
TBA solid	B3LYP	PBE	MP2	assignment
	249 (250)	239 (237)	249 (237)	C═S wagging
376	355 (356)	343 (340)	359 (341)	C═O and C−OH wagging
454	458 (459)	444 (440)	461 (438)	ring in-plane symmetric bending
494	519 (520)	500 (496)	508 (483)	ring in-plane asymmetric bending
525	580 (581)	563 (558)	583 (554)	$C_4-C_5-C_6$ bending
585	587 (588)	564 (559)	629 (598)	N_1-H out-of-plane bending
602	635 (636)	652 (646)	657 (625)	ring out-of-plane bending
612	680 (681)	678 (672)	695 (661)	N_3-H out-of-plane bending
716 wk	705 (706)	703 (697)	733 (696)	NH and C_5-H out-of-plane bending
n.d.	736 (736)	n.p.	n.p.	N_3-H and C_5-H out-of-plane bending
812	810 (811)	768 (761)	806 (766)	C_5-H out-of-plane bending
n.d.	931 (932)	907 (899)	943 (896)	C_4-N_3 and C_4-C_5 stretching
932	1003 (964)	977 (968)	1007 (957)	in-plane ring deformation
	1020 (981)	992 (983)	1017 (966)	in-plane ring deformation
1162	1147 (1103)	1116 (1106)	1170 (1112)	CS stretching and NH wagging in-plane
	1193 (1147)	1158 (1148)	1189 (1130)	C_5-H and OH wagging in-plane
	1221 (1172)	1187 (1176)	1237 (1176)	OH, CH, and NH wagging in-plane
1239	1270 (1221)	1233 (1222)	1296 (1231)	OH stretching and C_5-H wagging in-plane
1272	n.p.	n.p.	n.p.	?
1293	1365 (1312)	1306 (1294)	1365 (1297)	C_5-H, OH, and NH wagging in-plane
1350	1398 (1344)	1362 (1350)	1407 (1337)	$N_1-C_2-N_3$ asymmetric stretching
1403	1484 (1426)	1440 (1427)	1478 (1404)	C_6-N_1 stretching + N_3-H wagging
1436	n.p.	n.p.	n.p.	?
	1576 (1515)	1529 (1515)	1578 (1499)	C_6-N_1 stretching and N_1-H wagging
1648	1674 (1609)	1628 (1613)	1726 (1649)	C═C stretching
1720	1764 (1696)	1712 (1697)	1782 (1693)	C═O stretching
2873	n.p.	n.p.	n.p.	NH═O stretching
3096	3233 (3108)	3168 (3139)	3302 (3137)	C_5-H stretching
	3596 (3457)	3514 (3482)	3613 (3432)	N_3-H stretching
3450 w,wk	3614 (3474)	3531 (3499)	3631 (3449)	N_1-H stretching
	3827 (3679)	3718 (3685)	3865 (3672)	O−H stretching

[a] B3LYP, PBE, and MP2 calculations using the 6-311++G(2df,2pd) basis set in the gas phase; fundamental frequencies are given in parentheses and obtained from the calculated harmonic ones by employing the usual scaling factors of 1.0013 and 0.9614 for the lower and higher frequency ranges, respectively, for B3LYP, 0.9910 for PBE, and 0.9510 for MP2. [b] Notation: n.p. indicates not predicted; n.d. indicates not detected.

TABLE 4: Gas-Phase Energetics[a] of the Dimers Depicted in Chart 3

	6-31G(d)						6-311G(d,p)					
	CP corr	Δ_c(N1−SS)	total	Δ(N1−SS)	$\Delta_c$mon	Δmon	CP corr	Δ_c(N1−SS)	total	Δ(N1−SS)	$\Delta_c$mon	Δmon
N1−SS	−1626.03552	0.0	−1626.03831	0.0	−6.0	−7.8	−1626.31855	0.0	−1626.32068	0.0	−5.5	−6.9
N1−SO	−1626.03814	−1.6	−1626.04165	−2.1	−7.7	−9.9	−1626.32123	−1.7	−1626.32376	−1.9	−7.2	−8.8
N1−OO	−1626.04034	−3.0	−1626.04542	−4.5	−9.1	−12.3	−1626.32366	−3.2	−1626.32773	−4.4	−8.7	−11.3
N10−SS	−1625.99542	25.2	−1625.99830	25.1	−5.7	−7.5	−1626.28954	18.2	−1626.29182	18.1	−5.3	−6.7
N10−SS-assym	−1625.99860	23.2	−1626.00148	23.1	−7.7	−9.5	−1626.29257	16.3	−1626.29474	16.3	−7.2	−8.5
N10−SO	−1626.00277	20.6	−1626.00689	18.0	−10.3	−12.9	−1626.29698	13.5	−1626.29981	13.1	−9.9	−11.7
N10−SO-al	−1625.99409	26.0	−1625.99691	24.2	−4.9	−6.7	−1626.28825	20.4	−1626.29034	19.0	−4.5	−5.8
N10−OO	−1626.00245	20.8	−1626.00815	18.9	−10.1	−13.7	−1626.29670	13.7	−1626.30120	12.2	−9.8	−12.6
N10-alal	−1625.99458	25.7	−1626.00103	23.4	−5.2	−9.2	−1626.28783	19.3	−1626.29272	17.5	−4.2	−7.3
N10-keal	−1625.99887	23.0	−1626.00325	22.0	−7.9	−10.6	−1626.29306	16.0	−1626.29659	15.1	−7.5	−9.7

[a] Total energies (total) and counterpoise-corrected total energies (CP corr) for the 10 dimers depicted in Chart 3 are given in hartrees. Counterpoise-corrected (Δ_c) and uncorrected (Δ) relative energies with respect to the N1−SS dimer as well as counterpoise-corrected relative energies with respect to the N1 or N10 monomers (mon) are given in kcal/mol. Calculations performed using the B3LYP method with the basis sets shown.

calculated and theoretical spectrum can be even further reduced if a uniform shift of −15 nm is applied to the theoretical one (Figure 5b). The agreement now is evident, and the error between the experimental and theoretical results is within the precision observed for TD-DFT. Taking into account the molar absortivities given by Zucarello et al.[33] (N10, 265 nm, ϵ = 16 600 and N1, 283 nm, ϵ = 24 000), we obtain a concentration ratio very near to 1, [N10]/[N1] = 0.96, in agreement with our assumed hypothesis.

A final observation is that the UV−vis spectrum of TBA absorbed on gold nanoparticles differs from the one in methanol mainly in the relative intensity of the bands (Figure 4). As one can see from the relative contributions shown in Figure 5 for the theoretical simulation, this situation arises if the concentration of N10 increases at the expense of that of N1. In fact, the calculated ratio for the isomers absorbed on gold nanoparticles is [N10]/[N1] = 1.3.

NMR Spectra of TBA. The ^{1}H NMR spectrum of TBA in DMSO taken immediately after dissolution presents three clear signals at 12.1 ppm (s, 2H), 4.9 ppm (br, s, 1H), and 3.5 ppm (br, s, 1H), as already reported.[29] This implies that the spectrum cannot be due to the presence of only N1, since theoretically this isomer could produce only two signals in the NMR, both of them integrating to two. The alternative is then either N10 alone or a mixture of both. The ^{1}H NMR spectrum in DMSO for both isomers N1 and N10 was calculated at the PBE and B3LYP levels using the 6-311++G(2df,2pd) basis set. The calculations predict NH protons at 10.1 (N1), 9.9, and

TABLE 5: Most Interesting Transitions in the N10 Dimers[a]

			frequency[d]			intensity[e]	
dimer	ID[b]	transition[c]	harmonic	fundamental[f]	shift[g]	absolute (%)[h]	increase (%)[i]
N10−OO	1ν1	ν(OH)	3828	3679	−1	9	−5.2
	1ν2	ν(NH)	3613	3472	12	8	−1.4
	1ν3	ν(NH···O)	3291	3163	−297	100	
	1ν4	ν(CH)	3230	3104	2	1	0.2
	1ν5	ν(CO) + CNH bend	1749	1681	−41	74	0.0
	1ν6	coupled thioamide scissoring	1593	1531		59	
	1ν7	coupled OH + CNH bending	1520	1461		4	
	1ν8	coupled thioamide asym bending	1411	1356		1	
	1ν9	coupled thioamide scissoring	1160	1115		16	
N10−SO	2ν1	ν(OH)	3832/3828	3683/3679	+3/−1	7	−7.8
	2ν2	ν(NH)	3597/3609	3457/3468	−3/+8	6	−3.7
	2ν3	ν(NH···S)	3287	3159	−301	100	
	2ν4	ν(NH···O)	3198	3073	−387	59	
	2ν5	ν(CH)	3230/3224	3104/3098	+2/−4	0	−0.1
	2ν6	ν(CO) + CNH free bending	1791	1721	−1	34	−39.6
	2ν7	ν(CO) + CNH H-bond bending	1735	1667	−55	62	−37.8
	2ν8	ν(CC) + CNH H-bond bending	1686	1620		16	
	2ν9	ν(CC) + CNH free bending	1674	1609		32	
	2ν10	ν(CN) + CNH H-bond bending	1618	1555		40	
	2ν11	thioamide scissoring	1593	1531		40	
	2ν12	OH + NH H-bond bending	1512	1453		1	
	2ν13	OH + CH bending	1240	1192	23	14	
	2ν14	O′H′ bending	1227	1179	10	20	

[a] Obtained using the B3LYP/6-311G(d,p) chemical model; the normal mode vectors corresponding to the transitions are depicted in Figure SM1 in the Supporting Information. [b] Symbol used to identify the transition in Figure SM1. [c] Description of the main components of the normal mode. [d] In cm^{-1}. [e] As a percentage of the most intense transition. [f] Obtained from the harmonic frequencies by multiplying by the scale factor of 0.961. [g] With respect to the corresponding frequency in the isolated N10 isomer. [h] Percentage calculated with respect to the strongest transition in each dimer. [i] Relative increase or decrase in the signal with respect to the similar signal in the monomer.

9.8 (N10) ppm, with a ring H at 5.7 ppm and an OH proton at 8.1 ppm (N10), whereas the methylene protons of N1 are predicted at 3.7 ppm. One then sees clearly that a mixture of both isomers is improbable because of both the position of the signals and the number of protons they should integrate to. Consequently, one is forced to conclude that isomer N10 is the only one present in the freshly prepared DMSO solution. The discrepancy between the theoretically calculated chemical shifts and the experimental ones can be ascribed to the approximate nature of the calculations. However, an interesting comparison can be done between the theoretical results in DMSO and in vacuum. In fact, one sees that the solvent effect tends to coalesce the signals corresponding to the NH protons and to exchange the relative position of the OH and CH signals. Whereas the CH proton is more shifted in vacuum, it is less shifted than the OH proton in DMSO, in agreement with the more polar character of the latter.

^{13}C NMR of TBA in DMSO shows five signals for the four carbon atoms, at 82.8, 162.9, 166.8, 175.9, and 181.8 ppm, in accordance to earlier reports.[29,32] This indicates the existence of at least two isomers present in solution. It should be stressed that the ^{13}C NMR spectrum was accumulated over 2 days to obtain good signals, possibly allowing enough time for the N1⇌N10 equilibrium to take place. From the optimized geometries of the different isomers, the theoretical ^{13}C NMR spectra were obtained the same way as explained before; the calculated shifts for isomers N1 and N10 showed reasonable agreement with the experimental data (Table 10). According to these results, signals at 175.4 and 181.4 ppm are due to the thioamide group in both tautomers, whereas signals at 169.8 and 163.8 ppm are due to the keto−enol tautomeric forms; the signal at 88.3 ppm is due to the sp^2 C_5 state of isomer N10, whereas the predicted signal for the sp^3 C_5 state of isomer N1 at 41.4 ppm is masked by the one of DMSOs (signal calculated at 45.6 ppm). On the basis of these signal assignments, the experimental ratio [N10]/[N1] = 0.95. Notice that this value is the same as that obtained from the UV−vis spectrum in methanol, reinforcing our view that both isomers are in equilibrium.

Characterization of TBA-Capped Au Nanoparticles. TEM images of TBA-capped Au nanoparticles (Figure 7a) were obtained from the solid suspension; hence, they correspond to minute parts separated from the solid. Clearly, 3D structures between the nanoparticles are formed, indicating that TBA, once adsorbed, leaves free functional groups capable of interacting with other molecules, in this case, other TBA-capped Au nanoparticles. For this reason we have nicknamed them thistle particles. Three-dimensional structures among capped gold nanoparticles have also been observed for adsorbed 4-mercaptopyridine.[22] Particle sizes follow a lognormal distribution (Figure 7c), with a maximum corresponding to a diameter of 5.90 nm. EDS analysis of the solid formed during TBA-capped Au nanoparticles synthesis (Figure 7d) confirms the presence of N, O, and S atoms in the solid structure as minor components and the prevalence of the gold peaks, with an estimated mass representing 77% of the total sample.

Thermal gravimetric analysis of TBA-capped Au nanoparticles (Figure 6) indicates that TBA represents 25.4% of the total nanoparticles mass, with the remaining 74.6% accounted for by gold, in reasonable agreement with the value obtained by EDS analysis. No weight change was observed at 103 °C, indicating that no water associated to adsorbed TBA was present. The decomposition temperature[54] of isolated TBA is 235 °C, the process taking place in four steps. On the other hand, the thermal decomposition profile for adsorbed TBA involves only two steps, and the decomposition temperature is 339 °C. These figures are in accordance with a higher stability of TBA in the adsorbed state compared with the isolated form. The second step in the thermal decomposition of adsorbed TBA corresponds to a 35% weight drop, a figure that roughly accounts by for residue composed by one S and one N atom (theoretical value: 32%). This result provides evidence of a chelate configuration for adsorbed TBA involving these atoms.

TABLE 6: FTIR Signals for TBA in Methanol Solution and Comparison with the N1 and N10 Tautomers

experimental	calculated[a]				
	N1 tautomer		N10 tautomer		
TBA(MeOH)	PCM	cluster 2 Meth	PCM	cluster 2 Meth	assignment
455 w			430 w		OH torsion (solv)
	426 w	415w			sym ring stretching
519 w					
544 m					
619 m				618 w	out-of-plane sym NH wagging
634 sh			644 w		free NH wagging
654 w		656 w			Meth OH coupled NH wagging
671w		663 w/666 w			free NH wagging
683 w	681 m				out-of-plane sym NH wagging
720 m					
771 w			787 w		out-of-plane ring deformation
785 w			830 w		Meth OH torsion in $Meth_2TBA$
991 w		973 m			CH_2 rocking
1111 s	1089 s	1072 s	1104 m	1072 m	C═S stretching + thioamide scissoring
1168 m			1152 w		OH in-plane bending
1184 m	1190 m	1171 m			asym ring deformation in-plane
1214 w			1184 m	1244 m	NH + OH + CH in-plane bending
1261 w			1231 w	1210 w	CH in-plane bending
	1281 vs	1256 vs			sym ring deformation in-plane
1340 m	1343 m	1331 m			NH in-plane bending
1365−1381 w			1370 w	1336 w	asym ring deformation in-plane
1420 m			1418 vw	1400w/1404 m	OH + NH in-plane bending (solvent enhanced)
1458 m				1470 m	Meth bound OH bending
1510−1539 vs	1456 vs	1405 vs	1485 vs		thioamide scissoring
				1542 s	C═C stretching + OH, CH, and NH bending
1577,1605 m			1608 m/1573 vs	1553 m	C═O stretching + CNH bending
1635−1649 vs	1678 s/1653 vs	1580 s/1618 s			C═O stretching + CNH bending
2327 w/2361 s					dissolved CO_2 (exp 2349, calc 2357 cm^{-1})
				2665 vs	solvent-bound OH stretching
2853 ms		2738 s			CH_2···Meth (solvent)
	2938 w/2908 w	2857 vw	3033 w		CH stretching
2921 m	3100 s	2992 s/3006 m	3118 m/3136 m	3017/3039 w	NH stretching
3380 w/3443 m			3158 m		OH stretching
		3163 s/3265 vs		3204 s/3409 s	OH stretching of Meth in $Meth_2TBA$

[a] Gas-phase B3LYP/6-311++G(2df,2pd) calculations; fundamental frequencies were calculated from the harmonic ones by scaling them by a factor of 0.961.

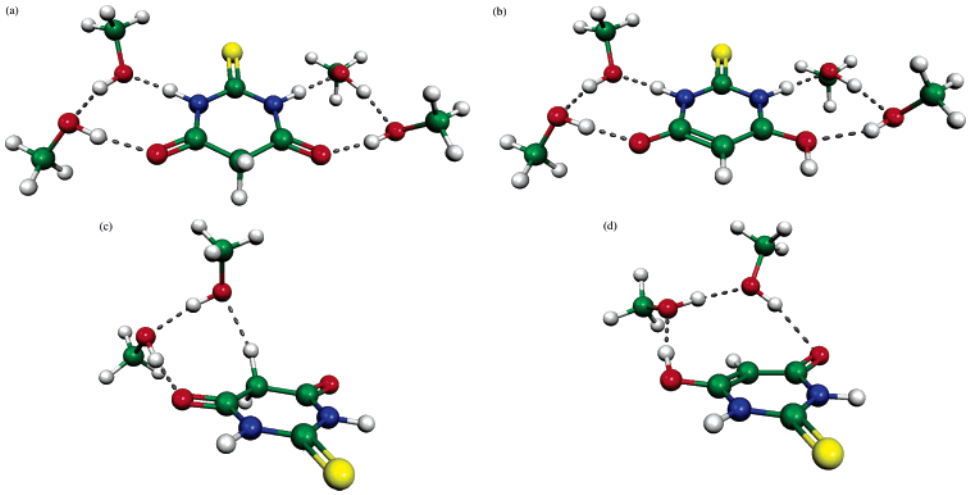

Figure 3. Optimum structures of some complexes of N1 (a and c) and N10 (b and d) with methanol.

The surface plasmon band for TBA-capped gold nanoparticles (Figure 7b) is located at 530.5 nm, corresponding to a particle diameter of 4.96 nm. In order to reconcile this value with that obtained by TEM analysis, the molecular size of TBA adsorbate was calculated on the basis of its optimized geometry. Taking into account the mean nanoparticles diameter measured by TEM (5.90 nm) and the calculated height of adsorbed TBA (0.50 nm), the actual mean diameter of gold nanoparticles alone is 5.90 − (2 × 0.50) = 4.90 nm, in nice agreement with that calculated from the surface plasmon band maximum.

Discussion

Molecular Structure of TBA in the Solid and in Solution. Organic molecules bearing mobile H atoms undergo tautomeric transformations. In particular, pyrimidines substituted at the 2 or 4 position by potentially tautomeric groups (OH or SH) exist

TABLE 7: Total and Relative Free Energies of the TBA (Meth)$_n$ Clusters (n = 2,4) Studied for Isomers N1 and N10

		gas phase		methanol (PCM)	
		total[a]	relative[b]	total[a]	relative[b]
N1	2 Meth	−1043.69485		−1043.71215	
	4 Meth	−1274.89812		−1274.88888	
N10	2 Meth	−1043.69013	3.0	−1043.70586	3.9
	4 Meth	−1274.87851	12.3	−1274.88747	0.9

[a] In hartrees. [b] In kcal/mol.

TABLE 8: FTIR Signals for TBA-Capped Gold Nanoparticles and Comparison with the N1 Isomer in Gas Phase[a,b]

experimental	theoretical	assignment
542 m		?
596 sh		?
617 vs		C−S single bond stretching
636 w		absorbed CO_2 bending (exp 667, calc 647 cm^{-1})
n.d.	652 w	free NH wagging
771w	779 w	out-of-plane ring deformation
827 w	830 w	residual Meth OH torsion
992 w		?
1103 s	1102 m	C═S stretching + thioamide scissoring
n.d.	1146 w	OH in-plane bending
1184 s	1173 m	OH + CH in-plane bending
1254 w	1220 w	CH in-plane bending
1340 w	1344 w	asym ring deformation in-plane
1385 m		adsorbed CO_2 stretching (exp 1349, calc 1321cm^{-1})
1418 w	1426 vw	OH in-plane bending (solvent enhanced)
1521 m	1515 vs	thioamide scissoring
1605 m	1609 m	C═O stretching
n.d.	1695 s	CNH bending
2341−2363 w		absorbed CO_2 stretching (exp 2340, calc 2357 cm^{-1})

[a] Gas-phase B3LYP/6-311++G(2df,2pd) calculations; fundamental frequencies were calculated from the harmonic ones scaling them by a factor of 0.961. [b] Notation: n.d. indicates not detected.

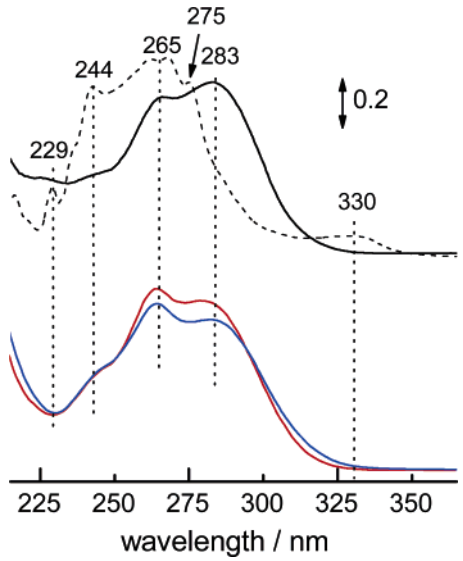

Figure 4. (top) UV−vis spectra of TBA in chloroform (dashed line) and in methanol (solid line). (bottom) Comparison of UV−vis spectra for TBA in methanolic solution with added $NaBH_4$ (red) and adsorbed onto Au nanoparticles (blue).

in lactam or thione forms in polar solutions.[15] TBA is no exception, and the presence of three potentially enolizable groups renders feasible the existence of a large number of tautomers. TBA and barbituric acid (BA) have been studied

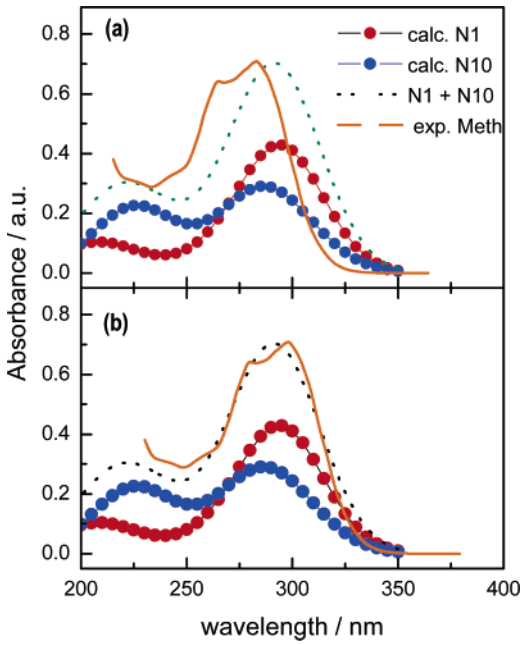

Figure 5. (a) Experimental and calculated UV-vis spectra in methanol. (b) The same spectra after a uniform shift of −15 nm was applied to the theoretical curves.

TABLE 9: Electronic Transitions in the UV−vis Range Calculated for N1 and N10 at Different Theoretical Levels[a]

	TDDFT/B3LYP			
isomer	6-31G(d)	6-311G(d,p)	6-311++G(2df,2pd)	aug-cc-pVTZ
N1	258 (0.39)	261 (0.40)	264 (0.40)	265 (0.40)
	222 (0.10)	221 (0.09)	222 (0.12)	223 (0.11)
	208 (0.06)	208 (0.06)	212 (0.08)	213 (0.08)
		192 (0.03)	208 (0.01)	209 (0.01)
			195 (0.04)	197 (0.04)
N10	267 (0.05)	267 (0.09)	273 (0.08)	275 (0.08)
	246 (0.26)	250 (0.27)	256 (0.24)	257 (0.22)
	229 (0.05)	230 (0.03)	248 (0.05)	250 (0.06)
	199 (0.19)	214 (0.01)	232 (0.02)	233 (0.02)
		199 (0.13)	224 (0.03)	226 (0.03)
			203 (0.19)	223 (0.01)
			200 (0.06)	205 (0.05)
			198 (0.02)	202 (0.19)

[a] Wavelengths are in nm; intensities in km/mol are given in parentheses.

TABLE 10: Experimental and Theoretical ^{13}C NMR Chemical Shifts of TBA in DMSO Solution (in ppm)

experimental	tautomer N1 (calc)[a]		tautomer N10 (calc)[a]	
39.5 (DMSO)	41.4	C_5		
82.1			88.3	C_5
162.7			163.8 + 164.8	$C_4 + C_6$
166.7	169.8	$C_4 + C_6$		
175.9			175.4	C_2
181.9	181.4	C_2		

[a] Carbon numbers are indicated in the respective isomers in Chart 1.

theoretically in recent times by Zuccarello et al.,[33] Ramondo et al.,[30] and Rathan and Ray[55] (only BA in this case). Zucarello et al.[33] employed the MP2 methods with a small 6-31G(d,p) basis set to study the 10 isomers depicted in Chart 1. Their results are qualitatively similar to those we obtained using more sophisticated methods, but some differences are worth noticing. According to Zucarello et al.,[33] N1 is the most stable isomer in gas phase and in PCM-simulated water solution. Due to the small basis set, N10 is calculated at 11.7 kcal mol^{-1} over N1 (internal energy without ZPE correction). The same value

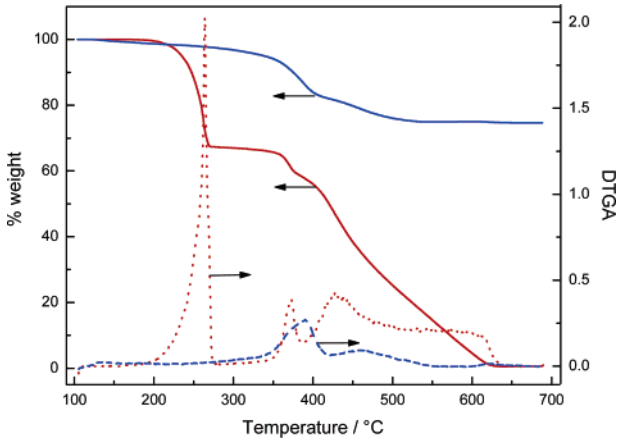

Figure 6. Thermal gravimetric (TGA, solid line) and differential thermal gravimetric (DTGA, dashed line) analyses of pure TBA (red) and TBA-capped gold nanoparticles (blue).

obtained by us at the larger MP2/6-311++G(2df,2pd) level is 9.0 kcal mol^{-1}, showing that the increase of the basis set plays in favor of N10 stabilization. The results obtained using the DFT methods of PBE and B3LYP are slightly different and smaller (7.7 and 7.8 kcal mol^{-1}, respectively), possibly because they include a larger part of the correlation energy than the MP2 calculations. The influence of the method and the basis set on the results can be appreciated in Table 1. With the use of the same basis set, B3LYP produces an energy of the N10 isomer about 2−3 kcal mol^{-1} lower than that of MP2. With the use of the same method, either B3LYP or MP2, the increase from a small to a large basis set provokes a decrease of about 40% in the energy difference between both isomers. Considering all facts, it seems however reasonable to say that N10 is about 8 kcal mol^{-1} less stable than N1 in gas phase at 0 K (ZPEs are reasonably similar for the two isomers, so that electronic and ZPE-corrected energy differences are similar).

Even from a qualitative point of view, however, the results of Zucarello et al.[33] and our solvation results differ markedly. Using water as a solvent Zucarello et al.[33] obtained a small stabilization of N10 (from 11.7 to 9.1 kcal mol^{-1}). In our case, however, and using methanol as solvent within the same PCM methodology, we report that N10 becomes more stable than N1 (−0.6, −0.2, and −0.1 kcal mol^{-1} at the PBE, B3LYP, and MP2 levels). There is also a difference in the method of calculation of the results. Zucarello et al.[33] included only the electronic energy for the solute and the free energy of interaction with the solvent (plus cavitation energy) in their calculations. Our results on the other side are all free energies, also including the solute in which statistical thermodynamic functions were calculated in the solvent. All our results agree that both isomers should be at equilibrium in methanol solution (unless forbidden by kinetic reasons), a result which is certainly relevant to explain the experimental data, which suggest both N1 and N10 to be in equal proportion in solution.

The PCM calculations show that the solvent effect is very important, even in a relatively innocuous solvent such as chloroform. A deeper analysis shows that this effect is mainly connected to the CH_2 group and the enolization of one of the C═O groups, exactly the path connecting isomers N1 and N10. In fact, one reaches this conclusion by analyzing the effect of specific solvation in the clusters of N1 and N10 with methanol molecules in comparison to the nonspecific solvation using the PCM method. In this last case, N10, which in gas phase was 8.9 kcal mol^{-1} less stable than N1, is now 0.6 kcal mol^{-1} more stable ($\Delta G°_{298}$ at the PBE/6-311++G(2df,2pd) level in both cases). If one now includes two methanol molecules linking the CH_2 group with O_7 in N1, one gets a not so marked but similar increase in the stability of N10 (from 8.9 to 3.0 kcal mol^{-1}) which is mostly unaffected by later including the PCM solvation energy (geometry optimization was performed in all cases). However, if the cluster is formed with methanol molecules linked to the amide portion of the molecule, the stability is actually decreased (from 8.9 to 12.3 kcal mol^{-1}), whereas including the PCM field later markedly increases the stability of N10 to 0.9 kcal mol^{-1} over N1. These data can be explained by assuming that preferential solvation by methanol will occur around the CH_2 "tail" of TBA and that solvent-assisted proton transfer will establish the N1−N10 equilibrium. Our present hypothesis is that whereas N10 is the predominant isomer in the solid (vide infra), an equilibrium between N1 and N10 is produced in polar solvents. The action of the solvent is responsible for the stabilization of the enol form of N10 by both stabilizing its charge distribution and helping the proton transfer from the methylene group. A detailed analysis of these reaction paths is under way and will eventually be published elsewhere. Meanwhile, notice that this theoretical analysis is in agreement with the presence of bands in the IR region assigned to solvent interaction with the CH_2 group.

Concerning the structure of TBA in solution and in the solid, a puzzling question remains. According to the experimental and theoretical data we obtained, there is no doubt of an equilibrium between N1 and N10 in solution; the solid-phase IR spectrum can be understood in terms of the presence of only N10. On the other side, N1 should be the most stable isomer in the gas phase. Regretfully, there is no report on the IR spectrum of gas phase TBA that we are aware of. However, the information about the TBA IR spectrum can be completed by comparing the gas-phase transitions calculated at the PBE, B3LYP, and MP2 levels with those of the FTIR spectrum measured by Ramondo et al.[30] for TBA into an Ar matrix (Table 11). These authors concluded that their calculations of the spectrum of the N1 isomer, done at the B3LYP/6-311++G(d,p) level, were in agreement with the experimental data. However, we observe several as yet unexplained discrepancies between the theoretical predictions and the experimental data. To better discuss these discrepancies we will refer to Figure 7(of the Ramondo et al.[30] paper and to the data in Table 11.

The first discrepancy observed refers to the intensity of the experimental band at 3415 cm^{-1}. This band is attributed by Ramondo et al.[30] to the ν(N−H) stretching and is calculated at 3587 (symmetric) and 3583 (asymmetric) cm^{-1}. These are harmonic values. Using our own calculations and scaling the harmonic values appropriately to obtain fundamental frequencies, we obtained the numbers shown in Table 11, all between 3430 and 3470 cm^{-1} and in reasonable agreement with experimental values. However, in both Ramondo et al.[30] calculations and our own, the intensities of these lines are relatively weak and should appear as *weak* bands in the experimental spectrum, not as *very strong* ones. The fact is noticeable in the simulated spectra, where the ν(N−H) symmetric and asymmetric stretching bands coalesce into a signal that is no more than 20% the value of the stronger ones between 1000 and 2000 cm^{-1}. Just for completeness, observe that N10 would give a similar band in this region (in both frequency and intensity).

The C═O stretching modes are observed experimentally at 1750 and 1740 cm^{-1}, in both cases as very strong bands. The symmetric and asymmetric ν(C═O) stretchings are predicted at 1727 and 1705 cm^{-1} by the PBE level, fairly well in

TABLE 11: Comparison between the FTIR Experimental Vibrational Transitions for TBA into an Ar Matrix and the Values Determined Theoretically in Vacuum Using Different Methods With the 6-311++G(2df,2pd) Basis Set for Isomers N1 and N10[a]

	Ramondo et al. (ref 30)			this work							
				isomer N1				isomer N10			
	description	B3LYP[b]	Ar matrix[c]	description	PBE	B3LYP	MP2	description	PBE	B3LYP	MP2
1								ν(OH)	3685 w	3678 w	3660 w
2	ν(NH)	3587 vw		ν(NH) symm	3472 vw	3449 vw	3436 vw	ν(NH)	3499 w	3473 w	3457 w
3	ν(NH)	3583 w	3415 vs	ν(NH) asymm	3468 w	3446 w	3433 w	νNH)	3483 vw	3457 w	3433 vw
4	ν(C═O)	1805 s	1750 vs	ν(C═O) + δ(NH) symm	1727 s	1732 s	1707 m	ν(C═O) + δ(NH)	1696 vs	1695 vs	1689 vs
5	ν(C═O)	1783 vs	1740 m	ν(C═O) + δ(NH) asymm	1705 vs	1711 vs	1691 s	νCC + δNH + δCH + δOH	1613 s	1609 s	1622 m
6	νNH + νCN + δCH$_2$	1542 vs	1513 vs					thioamide scissoring[d]	1516 vs	1515 vs	1515 vs
7	δCH$_2$	1423 vw	1501 vs	thioamide scissoring[d]	1470 s	1480 vs	1474 vs	νCN + δNH + δCH + δOH	1427 vw	1426 w	1418 vw
8	νNH + νCN+ δCH$_2$	1425 m	1416 m	CH$_2$ scissoring	1369 m	1368 m	1367 m				
9	ν(CN)	1381 vw	1371 w					νCN + δNH + δCH + δOH	1350 w	1344 w	1349 vw
10	CH$_2$ wagging	1312 vw	1357 vw	δ(NH) + δ(N'H')		1328 vw			1294 vw		
11			1335 m					ν(C═O) + δ(NH)+ δ(CH)	1222 w	1220 w	1221 w
12	ν(CN)	1334 vs	1330 vs	νCC + νCN + CH$_2$ scissoring	1284 vs	1287 vs	1298 vs	νCN + δNH + δCH + δOH	1176 w	1174 m	1182 w
13			1288 w	CH$_2$ twisting		1257 vw					
14			1279 vw	CH$_2$ twisting			1249 vw				
15			1260 vw								
16	νCN + δNH	1225 w	1220 w	in-plane ring deformation	1185 w	1182 w	1204 vw				
17	CH$_2$ twisting	1217 vw	1190 vw	CH$_2$ twisting		1168 vw		δCH + δOH	1147 w	1146 w	1138 vw
18	νC═S	1146 m	1145 vs	thioamide scissoring[d]	1108 w	1102 m	1122 m	thioamide scissoring[d]	1106 w	1102 m	1108 m
19	νCN + δNH	1024 vw						ν(C═S)	968 vw	965 vw	959 vw
20	CH$_2$ rocking	951 vw						NCC bending	899 vw	894 vw	902 vw
21	νCC + νCN	898 vw	934 vw					CH wagging	762 w	779 w	751 vw
22	νCC + νCN	885 vw						NH + CH wagging	672 vw	677 vw	668 w
23	γNH	708 w	699 s	NH wagging	712 w	711 w	687 w	NH wagging	646 vw	653 vw	632 vw
24	γNH	688 vw									

[a] Frequencies in cm^{-1}; intensities calculated as percentage of the strongest transition and coded according to the following ordering: vs, 75−100%; s, 50−75%; m, 20−50%; w, 10−20%; vw, 0−10%. The same procedure was used for coding the experimental and the theoretical transitions. [b] B3LYP/6-311++G(d,p) calculations. [c] Intensities reassigned according to the procedure described in (a); some of the frequencies not given by Ramondo et al.[30] were obtained directly from the recorded spectrum shown in their Figure 7. Since only the region below 1500 cm^{-1} is shown, only this region was reanalyzed. The frequencies and intensities reported by Ramondo et al.[30] were assumed for bands over 1500 cm^{-1}. [d] Thioamide scissoring involves a C═S stretching and simultaneous and symmetric NH and N′H′ bendings.

agreement with experiment. The similar bands in N10 are predicted at somewhat lower frequencies but near enough. And here now is another discrepancy. No explanation is given for the presence of two very close bands at 1513 and 1501 cm^{-1} in the experimental spectrum. Only one band appears theoretically at around 1480 cm^{-1}, which corresponds to the in-plane symmetric N−H bending. We propose that this band corresponds to the experimental one at 1501 cm^{-1} that Ramondo et al.[30] assign to δ(CH$_2$). The intensity of the δ(CH$_2$) band in both their calculations and ours is very small and should not be observed experimentally (in agreement with the fact that this vibration would scarcely change the dipole moment of the molecule). We believe that the band at 1513 cm^{-1} actually corresponds to the in-plane symmetric N−H bending of the second isomer N10, also a very strong band but shifted by a few cm^{-1} because of the nonequivalence of the oxygen atoms in N10. Finally, we assign the experimental strong band at 1416 cm^{-1} to the in-plane asymmetric N−H bending which appears at about 1370 cm^{-1} in the calculated spectrum.

The next strong band appears at 1330 cm^{-1} experimentally and between 1280 and 1300 cm^{-1} theoretically and corresponds to the symmetric C═N stretching as assigned by Ramondo et al.[30] The C═S stretching band appears at 1145 cm^{-1} experimentally and between 1100 and 1120 theoretically. However, this band is also *very strong* experimentally and only of *medium*-to-*weak* intensity in the calculations. And finally, the same happens with the band at 699 cm^{-1} in the experimental spectrum. In the calculations, this transition corresponds to the symmetric γ(N−H) but has a low intensity in comparison to other transitions. All in all, we do not think that the FTIR spectrum of TBA in Ar matrix is explained by either the N1 conformer alone, as assumed by Ramondo et al.,[30] or the superposition of the spectra of N1 and N10, as we assumed here. More work is needed to unravel this conundrum.

Spectroscopic studies of TBA methanolic solutions indicated the presence of both tautomers N1 and N10 in nearly equal concentrations. Good agreement has been obtained between the experimental results and theoretical calculations, taking into account this equilibrium, which we think is firmly supported by the data already presented. We do not have the theoretical data as yet to assert the speed of this transformation (basically the energy of activation in the solvent). However, the fact that the IR and UV spectra in methanolic solution indicate almost equal concentrations of both isomers and that the ^{1}H NMR spectrum of freshly prepared DMSO solutions can be explained by the presence of N10 exclusively, whereas the ^{13}C NMR spectrum requires the presence of both isomers to be explained, are all facts that suggest a fast equilibrium in methanol and a slow one in DMSO. Our hypothesis at the moment is that the isomeric equilibrium can be reached rapidly in methanol because of a solvent assisted proton transfer, whereas it is much slower in DMSO. The dissolution of TBA by methanol can be regarded as a multiple-step process. In the first place, the presence of methanol may disrupt intermolecular associations within N10 isomers, leading to solvated N10. Then, due to the similar stability of isomer N1 in solution, a tautomeric equilibrium is

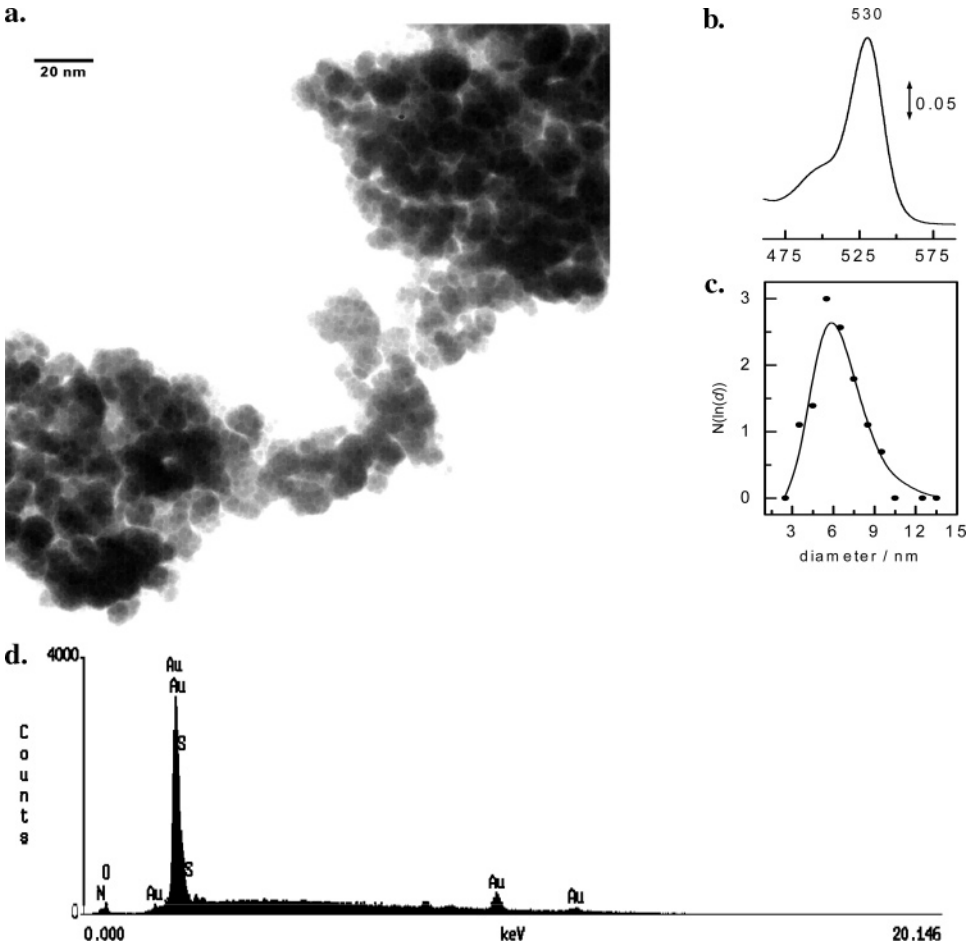

Figure 7. (a) TEM image, (b) surface plasmon band, (c) log-normal distribution of nanoparticle sizes, and (d) EDS spectra of TBA-capped Au nanoparticle aggregates.

established. Nuclear magnetic resonance results are in agreement with this scheme. Melting and vaporization of TBA would provide enough energy to overcome the barrier for transformation of N10 to N1, and this last tautomer would be the one present in larger quantities in gas phase due to its larger thermodynamic stability. The mixing with Ar and sudden deposition on the gold-plated copper coldfinger, as done experimentally, should deposit mostly N10 in the Ar matrix but should not completely exclude the N1 isomer.

IR spectra support the view that the structure of the absorbed isomer on the gold nanoparticles has the same general structure as that present in methanol. According to the previous theoretical analysis of the spectra, there is a larger ratio [N10]/[N1] for TBA absorbed on the nanoparticles than in methanolic solution. Although $NaBH_4$ employed for the synthesis of Au nanoparticles renders a basic medium, it appears insufficient to form TBA anions in significant amounts, since UV−vis spectra support the presence of the neutral isomers N1 and N10 in the conditions of Au nanoparticles synthesis. Bands located at 265 and 283 nm have inverted relative intensity values with respect to the methanolic TBA spectra, and a significant increase in the absorption intensity located at 244 nm is also observed (Figure 3b). The change in the relative intensities for the peaks at 265 and 283 nm is related to a concomitant change in the charge densities located at the S and C_2 atoms, respectively. On the other hand, since the molar extinction coefficient for the peak at 244 nm ($\epsilon = 8700$) is smaller than those of the bands at 265 nm ($\epsilon = 16\,600$) and 283 nm ($\epsilon = 24\,000$), the increase in intensity for the band at 244 nm (enol tautomer) should be considered indicative of an extensive equilibrium displacement toward the enolate form. In this sense, it is not surprising that the UV−vis spectrum of the methanolic suspension of TBA-capped gold nanoparticles shows the same features as those in methanolic TBA solutions with added $NaBH_4$, and hence, the electronic spectra provide strong evidence in favor of an enolate structure of adsorbed TBA.

To completely discard the idea that anions could be present in the solution once $NaBH_4$ is added, we studied the proton abstraction from both isomers N1 and N10. These are depicted in Chart 2. Anions A1 and A2 are produced by dissociation of a CH or an NH bond, respectively, in N1. Dissociation of the OH bond in N10 produces the same A1 anion as before, whereas dissociation of either one of the NH bonds produces A3 or A4. Finally, the dissociation of the remaining CH bond in N10 produces the anion A5. Four of these five structures have been studied before by Zucarello et al.,[33] and all of them were studied at the PBE/6-311++G(2df,2pd) level in this work in both vacuum and methanolic solution. The relative free energies of the five isomeric anions are collected in Table 12.

Anion A1, produced from isomer N1 by CH dissociation or from isomer N10 by OH dissociation, is the most stable one in both vacuum and solution by several kcal/mol, thus assuring that this will be the predominant species in basic media. The calculated ^{1}H NMR spectrum shows only two lines, at 5.0 (1H) and 9.1 (2H) ppm, corresponding to the CH and NH protons, respectively. The calculated ^{13}C NMR spectrum shows three lines at 86 (1H), 166 (2H), and 175 (1H) ppm, very near to those calculated for the N10 isomer itself (88, 165, 164, and 175 ppm, respectively). The UV−vis spectrum, calculated using TDDFT in methanol, gives a most intense signal at 258 nm,

TABLE 12: Free Energies at 298 K of the Mono and Dianions Derived from TBA Tautomers N1 and N10, Calculated at the PBE/6-311++G(2df,2pd) Level in Vacuum and Using the PCM Method To Simulate a Methanolic Solution[a]

	in vacuum		in methanol			in vacuum		in methanol	
monoanion	free energy[b]	ΔG^{o}_{298}[c]	free energy[b]	ΔG^{o}_{298}[c]	dianion	free energy[b]	ΔG^{o}_{298}[c]	free energy[b]	ΔG^{o}_{298}[c]
A1	−812.002124	0.0	−812.092050	0.0	DA1	−811.300311	0.0	−811.596447	0.0
A2	−811.983778	11.5	−812.075879	10.1	DA2	−811.319467	−12.0	−811.612518	−10.1
A3	−811.954851	29.7	−812.066989	15.7	DA3	−811.278645	13.6	−811.591874	2.9
A4	−811.984584	11.0	−812.079659	7.8	DA4	−811.287021	8.3	−811.594430	1.3
A5	−811.917416	53.2	−812.020472	44.9					

[a] Anions are identified in Chart 3. [b] In hartrees. [c] In kcal/mol.

SCHEME 1: Probable Mechanism of TBA Solvation in Polar Solvents and Further Adsorption onto Au Nanoparticles

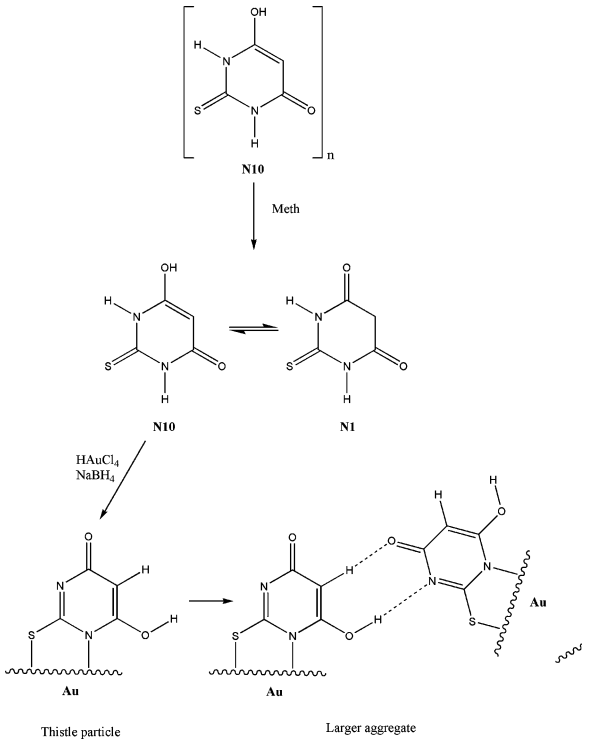

with weaker bands at 327, 271, 236, 231, and 222 nm. The intense band of A1 is co-incident with one of the bands of N10 itself, so it would not be observable by itself in the UV−vis region but may be the cause of the intensity increase in the band experimentally observed at 265 nm when going from a methanolic solution to another, including $NaBH_4$. Nonetheless, A1 cannot react as such with $AuCl_3$ to produce a sulfur bound complex, since the negative charge is distributed over the region of the oxygen atoms, not the sulfur.

TGA measurements confirmed the coordination of TBA to the surface through a chelate involving N and S atoms, a type of coordination specifically reported for Au(I)−thiobarbiturate complexes[26] as well as for other N-heterocyclic thiolates adsorbed onto gold.[56,57] This coordination is also supported by the almost complete disappearance of the C═S stretching band in the spectra of TBA-capped nanoparticles while the C═O bands remain as present in the methanol spectrum. Could this structure be formed by interaction with a dianion obtained from further deprotonation of A1?

To answer the previous question, the dianions of isomers N1 and N10 were investigated by optimizing the geometry of all the structures produced by the removal of two protons from N1 or N10 (also in Chart 2). Relative free energies are also shown in Table 12. As observed there, the dianion corresponding to deprotonation of one N and the O atoms in N10, with the negative charge distributed over sulfur, one of the N, and both O atoms, is the most stable structure, more stable than the corresponding one obtained from N1 (the two Hs over carbon) or those obtained from N10 keeping the proton on the O atom. This dianion, however, does not possess any resonant structure which could properly chelate Au and should be discarded. Thus, we conclude that neither the anion A1, which does not have the charge over sulfur, nor the most stable dianion DA2, which would not have a favorable structure for chelation of gold, can be the origin of the TBA coating of gold nanoparticles.

Thus, the only possibility remaining is the reaction of gold microclusters with the keto or enol tautomers in solution, by a redox reaction. The free energy in methanol favors reaction with the enol form, in agreement with the conclusion we have reached from the analysis of the experimental spectra.

Molecular Interactions among TBA-Capped Au Nanoparticles. TEM analysis supports the formation of 3D structures by aggregation of TBA-capped nanoparticles. The nature of Au−S bonding in 3D self-assembled monolayers is similar to those of Au(I) complexes;[23] hence, the X-ray structures of Au(I)−TBA complexes provide an interesting point of comparison.[26] These complexes, indeed, are able to form extensive intermolecular associations involving different kinds of H bonding, namely, N−H···O and C−H···O.[26]

Conclusions

The substituted mercaptopyrimidine 2-thiobarbituric acid (TBA) was chosen as the coating material for the modification of gold electrodes by a self-assembling procedure. The understanding of the adsorption of TBA onto gold made necessary the study of the molecular structure of the 10 possible TBA tautomers in the solid phase and in several solvents. To accomplish such a purpose, several experimental methodologies (IR, UV−vis, and NMR spectroscopies) were employed, aided by quantum chemical calculations at the DFT and MP2 levels for geometries, energetics, and spectra. TBA-capped gold nanoparticles were synthesized to study the adsorbed state of TBA. Particles of an average diameter of 5.90 nm were obtained, exhibiting high aggregation potential leading to larger clusters, presumably by multiple hydrogen bonding. Because of the similarity in the aggregation processes, we have nicknamed the TBA-coated gold nanoparticles thistle particles.

The results obtained in this work provide several new insights into the chemical structure of TBA and the effect of solvation on the prevalence of the different possible isomers. While N1 is the most stable tautomer in gas phase and nonpolar solutions, polar solvents stabilize a second tautomer, N10, that may be even more stable than N1 in methanol solution, a fact demonstrated here for the first time. Methanol, and presumably other protic solvents like water, causes an equilibrium to become established between N1 and N10, a fact reflected in the IR and UV spectra of methanolic solutions. Other solvents, like DMSO,

may help this equilibrium to become established over longer times, as was observed when the ^{13}C NMR spectrum of TBA solutions in DMSO was obtained.

The combined experimental and theoretical data favors the interaction of gold nanoparticles with the enol tautomer N10 in solution to form the thistle particles. A study of mono- and dianions of TBA suggests that the process does not occur by the interaction of $AuCl_3$ with the anion of TBA (which could exist in the basic conditions created by $NaBH_4$). TBA behaves similarly to Meldrum's acid[58] in that the methylene protons are very acidic and, in fact, methylene is the most acidic group in TBA, to the point that the most stable anion A1 (in both gas phase and methanol solution) is produced by the loss of one of these protons. A1, however, does not have the negative charge distributed over the sulfur atom and therefore cannot produce such a S−Au bond, as observed in the thistle particles. The same is true with respect to the most stable dianion (again in gas phase and in methanolic solution) DA2, which does not have an appropriate structure to give Au chelation, as deduced from the experimental observations. The proposed mechanism for this reaction is shown in Scheme 1. The structure of absorbed TBA derived from N10 exhibits a pair of polarizable protons pointing to the media, which may serve as anchor points for the network of hydrogen bonds which bind the thistle particles in larger aggregates.

The use of TBA-modified gold surfaces for redox protein attachment and electron-transfer studies is underway in our laboratory. The height of adsorbed TBA is 5 Å, which may favor the charge transfer between gold and the protein in the adiabatic regime, whereas the chelate configuration of the adsorbed entity led to a higher stability of the structure, as deduced from thermal gravimetric analysis. Moreover, the exposed functional groups of adsorbed TBA would interact favorably with several protein residues. Results of electrochemical impedance spectroscopy and quartz crystal microbalance are in accordance with these ideas and will be reported shortly.

Acknowledgment. This work was financially supported by CSIC (UdelaR) project awarded to E.M. and PEDECIBA (PNUD/URU/97/016). The authors thank Prof. Gustavo Scuseria for valuable advice concerning the accuracy of TD-DFT, Dr. G. Oblomov for his experimental suggestions, the Advanced Biomedical Computing Center of the National Cancer Institute (Frederick, MD for the generous allocation of computing time, and Dr. Raúl E. Cachau for fruitful discussions concerning the subject of this paper.

Supporting Information Available: Figure SM1, most significant vibrational modes of $(N1)_2$ and $(N10)_2$ dimers; Table SM1, gas-phase total free energies for isomers N1 to N10 using B3LYP and MP2 with several basis sets of increasing sophistication; Table SM2, gas-phase and solvation total free energies for isomers N1 to N10 using different methods and the large 6-311++G(2df,2pd) basis set. This material is available free of charge via the Internet at http://pubs.acs.org.

References and Notes

(1) Terrettaz, S.; Cheng, J.; Miller, C. J. *J. Am. Chem. Soc.* **1996**, *118*, 7857.

(2) Yamamoto, H.; Liu, H.; Waldeck, D. H. *Chem. Commun.* **2001**, 1032.

(3) Leopold, M. C.; Bowden, E. F. *Langmuir* **2002**, *18*, 2239.

(4) Gooding, J. J.; Meams, F.; Yang, W.; Liu, J. *Electroanalysis* **2003**, *15*, 81.

(5) Khoshtariya, D. E.; Wei, J.; Liu, H.; Yue, H.; Waldeck, D. H. *J. Am. Chem. Soc.* **2003**, *125*, 7704.

(6) Avila, A.; Gregory, B. W.; Niki, K.; Cotton, T. M. *J. Phys. Chem. B* **2000**, *104*, 2759.

(7) Niki, K.; Sprinkle, J. R.; Margoliash, E. *Bioelectrochemistry* **2002**, *55*, 37.

(8) Sawaguchi, T.; Mizutani, F.; Taniguchi, I. *Langmuir* **1998**, *14*, 3565.

(9) Doneux, T.; Buess-Herman, C.; Lipkowski, J. *J. Electroanal. Chem.* **2004**, *564*, 65.

(10) Cai, C. X. *J. Electroanal. Chem.* **1995**, *393*, 119.

(11) Lamp, B. D.; Hobara, D.; Porter, M. D.; Niki, K.; Cotton, T. M. *Langmuir* **1997**, *13*, 736.

(12) Taniguchi, I.; Yoshimoto, S.; Nishiyama, K. *Chem. Lett.* **1997**, 353.

(13) Sawaguchi, T.; Mizutani, F.; Yoshimoto, S.; Taniguchi, I. *Electrochim. Acta* **2000**, *45*, 2861.

(14) Jun, Y. Y.; Beng, K. S. *Electrochem. Commun.* **2004**, *6*, 87.

(15) Stoyanov, S.; Petkov, I.; Antonov, L.; Stoyanova, T.; Karagiannidis, P.; Aslanidis, P. *Can. J. Chem.* **1990**, *68*, 1482.

(16) Pang, Y. S.; Hwang, H. J.; Kim, M. S. *J. Mol. Struct.* **1998**, *441*, 63.

(17) Martos-Calvente, R.; de la Peña O'Shea, A.; Campos-Martin, J. M.; Fierro, J. L. G. *J. Phys. Chem. A* **2003**, *107*, 7490.

(18) Huang, X.; Li, C.; Jiang, S.; Wang, X.; Zhang, B.; Liu, M. *J. Am. Chem. Soc.* **2004**, *126*, 1322.

(19) Muthu, S.; Vittal, J. J. *Cryst. Growth Des.* **2004**, *4*, 1181.

(20) Lewis, T. C.; Tocher, D. A.; Price, S. L. *Cryst. Growth Des.* **2004**, *4*, 979.

(21) Lapinski, L.; Nowak, M. J.; Kwiatkowski, J. S.; Leszczynski, J. *J. Phys. Chem. A* **1999**, *103*, 280.

(22) Zhang, H.-L.; Evans, S. D.; Henderson, J. R.; Miles, R. E.; Shen, T. *J. Phys. Chem. B* **2003**, *107*, 6087.

(23) Bourg, M. C.; Badia, A.; Lennox, R. B. *J. Phys. Chem. B* **2000**, *104*, 6562.

(24) Hasan, M.; Bethell, D.; Brust, M. *J. Am. Chem. Soc.* **2002**, *124*, 1132.

(25) Hostetler, M. J.; Stokes, J. J.; Murray, R. W. *Langmuir* **1996**, *12*, 3604.

(26) Hunks, W. J.; Jennings, M. C.; Puddephatt, R. J. *Inorg. Chem.* **2002**, *41*, 4590.

(27) Mirsky, V. M..; Hirsch, T.; Piletsky, S. A.; Wolfbeis, O. S. *Angew. Chem., Int. Ed.* **1999**, *38*, 1108.

(28) Peng, Z.; Walther, T.; Keinermanns, K. *Langmuir* **2005**, *21*, 4249.

(29) García Tasende, M. S.; Suárez Gimeno, M. I.; Sánchez, A.; Casas, J. S. *J. Organomet. Chem.* **1990**, *390*, 293.

(30) Ramondo, F.; Pieretti, A.; Gontrani, L.; Bencivenni, L. *Chem. Phys.* **2001**, *271*, 293.

(31) Carroll, F. I.; Philip, A. *J. Med. Chem.* **1976**, *19*, 521.

(32) Pegg, R. B.; Shahidi, F.; Jablonski, C. R. *J. Agric. Food Chem.* **1992**, *40*, 1826.

(33) Zucarello, F.; Buemi, G.; Gandolfo, C.; Contino, A. *Spectrochim. Acta, Part A* **2003**, *59*, 139.

(34) Tripathi, G. N. R.; Clements, M. *J. Phys. Chem. B* **2003**, *107*, 11125.

(35) Møller, C.; Plesset, M. S. *Phys. Rev.* **1934**, *46*, 618.

(36) Koch, W.; Holthausen, Max C. *A Chemist's Guide to Density Functional Theory*, 2nd ed.; Wiley-VCH: Weinheim, Ger., 2001.

(37) (a) Perdew, J. P.; Burke, K.; Ernzerhof, M. *Phys. Rev. Lett.* **1996**, *77*, 3865. (b) Perdew, J. P.; Burke, K.; Ernzerhof, M. *Phys. Rev. Lett.* **1997**, *78*, 1396.

(38) (a) Becke, A. D. *J. Chem. Phys.* **1993**, *98*, 5648. (b) Becke, A. D. *Phys. Rev. A: At., Mol., Opt. Phys.* **1988**, *38*, 3098. (c) Lee, C.; Yang, W.; Parr, R. G. *Phys. Rev. B: Condens. Matter* **1988**, *37*, 785. (d) Miehlich, B.; Savin, A.; Stoll, H.; Preuss, H. *Chem. Phys. Lett.* **1989**, *157*, 200.

(39) (a) Hehre, W. J.; Radom, L.; Schleyer, P. v. R.; Pople, J. A. *Ab Initio Molecular Orbital Theory*; Wiley: New York, 1986. (b) Foresman, J. B.; Frisch, Æ. *Exploring Chemistry with Electronic Structure Methods*, 2nd ed.; Gaussian, Inc.: Pittsburgh, PA, 1996.

(40) (a) Woon, D. E.; Dunning, T. H., Jr. *J. Chem. Phys.* **1993**, *98*, 1358. (b) Kendall, R. A.; Dunning, T. H., Jr.; Harrison, R. J. *J. Chem. Phys.* **1992**, *96*, 6796. (c) Dunning, T. H., Jr. *J. Chem. Phys.* **1989**, *90*, 1007. (d) Peterson, K. A.; Woon, D. E.; Dunning, T. H., Jr. *J. Chem. Phys.* **1994**, *100*, 7410. (e) Wilson, A.; van Mourik, T.; Dunning, T. H., Jr. *J. Mol. Struct. (THEOCHEM)* **1997**, *388*, 339. (f) Davidson, E. R. *Chem. Phys. Lett.* **1996**, *260*, 514.

(41) (a) Tomasi, J.; Mennucci, B.; Cammi, R. *Chem. Rev.* **2005**, *105*, 2999. (b) Mennucci, B.; Tomasi, J. *J. Chem. Phys.* **1997**, *106*, 5151. (c) Mennucci, B.; Cancès, E.; Tomasi, J. *J. Phys. Chem. B* **1997**, *101*, 10506. (d) Cammi, R.; Mennucci, B.; Tomasi, J. *J. Phys. Chem. A* **1999**, *103*, 9100. (e) Cammi, R.; Mennucci, B.; Tomasi, J. *J. Phys. Chem. A* **2000**, *104*, 5631. (f) Cossi, M.; Scalmani, G.; Rega, N.; Barone, V. *J. Chem. Phys.* **2002**, *117*, 43, and references therein.

(42) (a) Stratmann, R. E.; Scuseria, G. E.; Frisch, M. J. *J. Chem. Phys.* **1998**, *109*, 8218. (b) Bauernschmitt, R.; Ahlrichs, R. *Chem. Phys. Lett.* **1996**, *256*, 454. (c) Casida, M. E.; Jamorski, C.; Casida, K. C.; Salahub, D. R. *J. Chem. Phys.* **1998**, *108*, 4439.

(43) (a) Gauss, J. *J. Chem. Phys.* **1993**, *99*, 3629. (b) Gauss, J. *Phys. Chem. Chem. Phys.* **1995**, *99*, 1001.

(44) (a) Ditchfield, R. *Mol. Phys.* **1974**, *27*, 789. (b) Dodds, J. L.; McWeeny, R.; Sadlej, A. J. *Mol. Phys.* **1980**, *41*, 1419. (c) Wolinski, K.; Hilton, J. F.; Pulay, P. *J. Am. Chem. Soc.* **1990**, *112*, 8251.

(45) (a) Boys, S. F.; Bernardi, F. *Mol. Phys.* **1970**, *19*, 553. (b) Simon, S.; Duran, M.; Dannenberg, J. J. *J. Chem. Phys.* **1996**, *105*, 11024.

(46) Frisch, M. J.; Trucks, G. W.; Schlegel, H. B.; Scuseria, G. E.; Robb, M. A.; Cheeseman, J. R.; Montgomery, Jr., J. A.; Vreven, T.; Kudin, K. N.; Burant, J. C.; Millam, J. M.; Iyengar, S. S.; Tomasi, J.; Barone, V.; Mennucci, B.; Cossi, M.; Scalmani, G.; Rega, N.; Petersson, G. A.; Nakatsuji, H.; Hada, M.; Ehara, M.; Toyota, K.; Fukuda, R.; Hasegawa, J.; Ishida, M.; Nakajima, T.; Honda, Y.; Kitao, O.; Nakai, H.; Klene, M.; Li, X.; Knox, J. E.; Hratchian, H. P.; Cross, J. B.; Bakken, V.; Adamo, C.; Jaramillo, J.; Gomperts, R.; Stratmann, R. E.; Yazyev, O.; Austin, A. J.; Cammi, R.; Pomelli, C.; Ochterski, J. W.; Ayala, P. Y.; Morokuma, K.; Voth, G. A.; Salvador, P.; Dannenberg, J. J.; Zakrzewski, V. G.; Dapprich, S.; Daniels, A. D.; Strain, M. C.; Farkas, O.; Malick, D. K.; Rabuck, A. D.; Raghavachari, K.; Foresman, J. B.; Ortiz, J. V.; Cui, Q.; Baboul, A. G.; Clifford, S.; Cioslowski, J.; Stefanov, B. B.; Liu, G.; Liashenko, A.; Piskorz, P.; Komaromi, I.; Martin, R. L.; Fox, D. J.; Keith, T.; Al-Laham, M. A.; Peng, C. Y.; Nanayakkara, A.; Challacombe, M.; Gill, P. M. W.; Johnson, B.; Chen, W.; Wong, M. W.; Gonzalez, C.; and Pople, J. A.; *Gaussian 03*, revision C.02*;* Gaussian, Inc.: Wallingford CT, 2004.

(47) Brust, M.; Walker, A.; Bethrell, D.; Schiffrin, D. J.; Whyman, R. *J. Chem. Soc., Chem. Commun.* **1994**, 801.

(48) Bidermann, G.; Sillén, L. G. *Ark. Kemi* **1953**, *5*, 425.

(49) Liberti, A.; Light, I. S. *J. Chem. Educ.* **1962**, *39*, 236.

(50) Gans, P.; Sabatini, A.; Vacca, A. *Talanta* **1996**, *43*, 1739.

(51) Alderighi, L.; Gans, P.; Ienco, A.; Peters, D.; Sabatini, A.; Vacca, A. *Coord. Chem. Rev.* **1999**, *184*, 311.

(52) Rasband, W. *ImageJ*, version 1.30v; U. S. National Institutes of Health: Bethesda, MD.

(53) Mayo, D. W.; Miller, F. A.; Hannah, R. W. *Course Notes on the Interpretation of Infrared and Raman Spectra*; J. Wiley & Sons: Hoboken, NJ, 2003; p 237.

(54) Decomposition temperature is considered to be that corresponding to a weight decrease of 5%.

(55) Rathan, S.; Ray, N. K. *J. Mol. Struct. (Theochem)* **2003**, *634*, 83.

(56) Hao, L.; Lachicotte, R. J.; Gysling, H. J.; Eisenberg, R. *Inorg. Chem.* **1999**, *38*, 4616.

(57) Tzeng, B. C.; Chan, C. K.; Cheung, K. K.; Che, C. M.; Peng, S. M. *J. Chem. Soc., Chem. Commun.* **1997**, 135.

(58) Nakamura, S.; Hirao, H.; Ohwada, T. *J. Org. Chem.* **2004**, *69*, 4309.